DOI 10.1007/s11182-018-1288-7

Russian Physics Journal, Vol. 60, No. 10, February, 2018 (Russian Original No. 10, October, 2017)

THE EFFECT OF ION IRRADIATION ON NANOCRYSTALLIZATION AND SURFACE RELIEF OF A RIBBON FROM $Fe_{72.5}Cu_1Nb_2Mo_{1.5}Si_{14}B_9$ ALLOY

I. Yu. Romanov,[1] N. V. Gushchina,[1] V. V. Ovchinnikov,[1,2] F. F. Makhinko,[1] A. V. Stepanov,[1] A. I. Medvedev,[1] Yu. N. Starodubtsev,[2,3] V. Ya. Belozerov,[3] and B. A. Loginov[4]

UDC 539.12.043:(536.425+537.622.4)

Using the methods of X-ray diffraction and atomic force microscopy, the process of crystallization of an amorphous $Fe_{72.5}Cu_1Nb_2Mo_{1.5}Si_{14}B_9$ *alloy irradiated with accelerated* Ar^+ *ions is investigated. It is found out that an irradiation by the* Ar^+ *ions with the energy 30 keV at the ion current density 300* $\mu A/cm^2$ *(fluence* $3.75 \cdot 10^{15}$ cm^{-2}*, irradiation time ~2 s, ion-beam short-duration heating up to 350°C, which is 150°C lower than the thermal crystallization threshold) results in a complete crystallization of this amorphous alloy (throughout the bulk of a 25 μm ribbon) followed by precipitation of solid solution crystals of* α-Fe(Si), *close in its composition to* $Fe_{80}Si_{20}$, *stable phase of* Fe_3Si, *and metastable hexagonal phases. By the methods of atomic force and scanning tunneling microscopy it is shown that nanocrystallization caused by ion irradiation is accompanied by surface relief changes both on the irradiated and unirradiated sides of the* $Fe_{72.5}Cu_1Nb_2Mo_{1.5}Si_{14}B_9$ *alloy ribbon at the depth exceeding by a factor of* 10^3 *that of the physical ion penetration for this material. The data obtained, taking into account a significant temperature decrease and multiple acceleration of the crystallization process, serve an evidence of the radiation-dynamic influence of accelerated ions on the metastable amorphous medium.*

Keywords: ion irradiation, magnetically soft alloy, crystallization, nanocrystalline structure, X-ray diffraction, atomic force microscopy.

INTRODUCTION

At present time for creating nanomaterials of different functional applications a variety of material-processing methods have been developed, such as superfast liquid quenching, high-pressure shear, equal-channel angular pressing (followed by heat treatment) [1–3], formation (spraying, deposition, etc.) of nanolayers of varied thicknesses and compositions [4, 5], etc. Moreover, there are a number of compaction technologies for production of three-dimensional articles from nanopowders [6–8].

With an advent of technological ion sources ensuring generation of high-power ion beams of different elements [9, 10], including the beams with a large cross-section area, new prospects for surface amorphization and nanostructuring of functional materials have been opened for the formation of predetermined functional properties.

[1]Institute of Electrophysics of the Ural Branch of the Russian Academy of Sciences, Ekaterinburg, Russia, e-mail: ivan.ekb@rambler.ru; guscha@rambler.ru; viae05@rambler.ru; ffm1979@mail.ru; stepanovav@mail.ru; medtom@iep.uran.ru; [2]B. N. Yeltsin Ural Federal University, Ekaterinburg, Russia, e-mail: yunstar@mail.ru; [3]Gammamet Research and Production Enterprise, Ekaterinburg, Russia, e-mail: gammamet@mail.ur.ru; [4]National Research University of Electronic Technology (MIET), Zelenograd, Russia, e-mail: b-loginov@mail.ru. Translated from Izvestiya Vysshikh Uchebnykh Zavedenii, Fizika, No. 10, pp. 157–165, October, 2017. Original article submitted August 19, 2017.

As concerns the articles produced from metals and their alloys, considering the small value of the free-path length of medium-energy (10–100 keV) ions in metal materials, which constitute fractions of a micron, initially only the contact-chemical and tribological properties were modified. More recently, a number of methods were developed for modification of electrical, magnetic, and mechanical properties (including those of amorphous, mono-, macro-, micro-, meso-, and nanocrystalline materials) [11–14]. For targeted modification of surface and bulk properties of materials use is made of so-called radiation-dynamic effects [14]. These are nanoscale effects associated with the generation and propagation of post-cascade shock waves (formed in the course of evolution of dense cascades of atomic displacements capable of initiating structural-phase transformations at their fronts). In practice, it is possible to modify the properties of lengthy subsurface layers whose thickness in certain cases reaches a few tens of millimeters (i. e., by a factor of 10^4–10^5 and more exceeds the average projective ion range in matter) [13, 14].

For instance in [12] the properties of amorphous and nanocrystalline magnetically soft materials were modified with the beams of accelerated argon ions. The reversal magnetization losses in the initially amorphous (nanocrystalline after a standard treatment) ribbons of the $Fe_{73.5}Cu_1Nb_3Si_{13.5}B_9$ composition with the thickness up to 0.1 mm after irradiation with low doses (10^{15}–10^{16} cm^{-2}) of Ar^+ ions were reduced due to the formation of a special material structure on average by 10%. An RF patent was obtained for the method of improving the properties of magnetically soft materials [15]. In [16, 17] the authors reported the effects of decreasing the recrystallization temperatures in pure Fe, Cu and Mo, subjected to severe plastic deformation, improving the homogeneity degree of the nanostructure formed in them in the course of ion bombardment.

Despite the facts of the promising applications of the methods for ion-beam treatment for modification of material properties (including modification due to the formation of surface and three-dimensional nanostructures), the physical nature of the processes taking place during this treatment is still insufficiently studied. Therefore, it is of interest to further study nanoscale dynamic effects under ion bombardment. The methods of controlling the parameters of nanosized structural components could form the basis of new industrial technologies for improving the electrical, magnetic, mechanical, durability-related, and other properties of functional materials.

The purpose of this work is to study the process of crystallization of the amorphous $Fe_{72.5}Cu_1Nb_2Mo_{1.5}Si_{14}B_9$ alloy ribbons under the action of accelerated Ar^+ ions with the energy 30 keV.

1. MATERIAL AND EXPERIMENTAL PROCEDURE

The $Fe_{72.5}Cu_1Nb_2Mo_{1.5}Si_{14}B_9$ alloy belongs to a group of alloys based on the Fe–Cu–Nb– Si–B composition. Such alloys, also referred to as finemets, [18, 19], demonstrate low magnetic reversal losses and possess high saturation magnetic induction. Their application allows considerably decreasing the weight and dimensions of electronic devices. The ribbons from the $Fe_{72.5}Cu_1Nb_2Mo_{1.5}Si_{14}B_9$ alloy measuring 25 μm in thickness and 10 mm in width were manufactured by the Gammamet research and production enterprise (Ekaterinburg, Russia). They were produced by superfast liquid quenching and were kept at room temperature in the initially amorphous metastable state.

The irradiation of the ribbons was carried out in an ILM-1 ion implanter equipped with a Pulsar-1M ion source relying on a low-pressure glow discharge with a cold cathode [20]. This ion source allows forming ion beams of cylindrical configuration with the cross-section area 100 cm^2 and the ion current density j from 50 to 500 μA/cm^2 (in a continuous mode) , which is constant across the section, at the accelerating voltages U from 5 to 40 kV.

The ribbons were cut to form individual specimens 60 cm long. A special device was used to irradiate them, which was moving in the implanter chamber and had a collector for the specimens, which allowed the irradiated specimens to be displaced under the ion beam at a given velocity from 1 to 5 cm/s. A slit collimator was installed on the source to form a ribbon ion beam with the cross section area 2×10 cm^2.

The temperature of (one or several) moving specimens in the course of their irradiation was monitored with a chromel-alumel thermocouple (welded to the witness-ribbon being moved together with the other specimens), which was switched to a monitoring system based on the ADAM-4000 modules (Advantech, USA). The temperature of part of the ribbon reached its maximum values within a few seconds due to ion-beam heating and, due to high heat conduction, rapidly cooled to below 40°C.

The following regime was used to irradiate the initially amorphous specimens: E = 30 keV, j = 300 μA/cm^2. The velocity of ribbon displacement with respect to the beam was 1 cm/s (a simple calculation shows this to correspond to the fluence $F = 3.75 \cdot 10^{15}$ cm^{-2}). The dwell time under the beam for every point on the ribbon surface for this displacement velocity was equal to 2 s. The experimentally measured temperature of specimen heating by the ion beam in the course of short-duration irradiation did not exceed (350 ± 10)°C. The specimens were irradiated from the contact side of the ribbon, i.e., the one contacting the drum during quenching.

It was assumed to compare the results of the influence of ion-beam irradiation and ordinary heating on the initial (produced by superfast quenching) ribbons of the $Fe_{72.5}Cu_1Nb_2Mo_{1.5}Si_{14}B_9$ alloy. To this end, along with irradiation the ribbons were subjected to annealing in the furnace in air at the temperatures from 450 to 570°C for 1 h. In addition, in order to estimate the stability of the state produced by irradiation, the irradiated specimens were also annealed at similar conditions.

The investigations of the influence of Ar^+ ions with the energy 30 keV and that of the ordinary heating on the process of nanocrystallization of the $Fe_{72.5}Cu_1Nb_2Mo_{1.5}Si_{14}B_9$ alloy were performed by the method of XRD analysis. Furthermore, with a purpose of identifying the role of long-range effects (for short irradiation times) at the distances exceeding the projective ion range by three orders of magnitude, we investigated the relief changes on the irradiated and unirradiated ribbon surfaces using scanning probe microscopy.

The XRD patterns were taken both from the irradiated and initial surfaces in a D8 DISCOVER diffractometer (Bruker, Germany) in the Cu$K_{\alpha 1,2}$ emission, using the Bragg – Brentano diffracted-beam graphite-monochromator focusing geometry. The results were processed using a TOPAS-3 full-profile analysis program. The volume fraction of the amorphous component was estimated from the relative contribution of two diffusion peaks in the diffraction patterns. In order to estimate the average crystallite size, the Scherrer method was used (applying the width of the diffraction maximum at a half height) with the shape correction factor 0.89.

The scanning probe microscopic investigations were carried out in an SMM-2000 scanning probe microscope (Proton enterprises, Zelenograd), which ensures operation both in the atomic-force and tunneling modes. In the former case, a flexible probe interacts directly with the surface and its deviation from the initial state characterizes the surface relief changes. In the latter case, the spatial position of the conducting probe is determined by the presence of tunneling current between the probe and the surface. A comparative analysis of the initial amorphous specimens with those irradiated in the above-mentioned regime is performed. The relief characteristic parameters used in this study were average surface roughness R_a and the relative profile length L_0 (the ratio of the length of the profile line to the length of the profile projection), which is a characteristics of the surface development. The measurements were performed on both sides (irradiated and unirradiated).

2. EXPERIMENTAL RESULTS AND DISCUSSION

Figure 1 presents the diffraction patterns taken from the initial $Fe_{72.5}Cu_1Nb_2Mo_{1.5}Si_{14}B_9$ alloy specimens in the states after quenching (*a*) and after subsequent heat treatment 570°C for 1 h (*b*). The diffraction patterns from the ribbon in the initial quenched state contains only the amorphous halo. After the heat treatment of the ribbon at the temperature higher than 480°C, in addition to the amorphous halo there are reflections of the crystal phases. Note that the center of the halo tends to displacing towards small angles with increasing annealing temperature.

An analysis of the diffraction patterns from the initially quenched specimen after its heat treatment at the temperatures from 480 to 570°C for 1 h (Table 1, Fig. 1*b*) demonstrate that one of the crystal phases formed is α-Fe – based solid solution and that the observed value of the crystal lattice period 0.2844 nm corresponds to the $Fe_{80}Si_{20}$ composition. The second crystal phase is Fe_3Si with the crystal lattice period 0.5660 nm. An estimation of the average grain size (CSRs) using the Scherrer method produced the value 17 nm for the α-Fe(Si) solid solution crystals and 19 nm for Fe_3Si.

After irradiation of the specimens with Ar^+ ions in the above-described regime there is no halo on the diffraction patterns, and the diffraction lines correspond to a multiphase crystal structure (Fig. 2*a*). As a result of further heat treatment of the irradiated specimen at 570°C for 1 h the diffraction pattern hardly changes (Fig. 2*b*). An analysis has shown that part of the spectral lines correspond to the crystal phases similar to those revealed in the case of

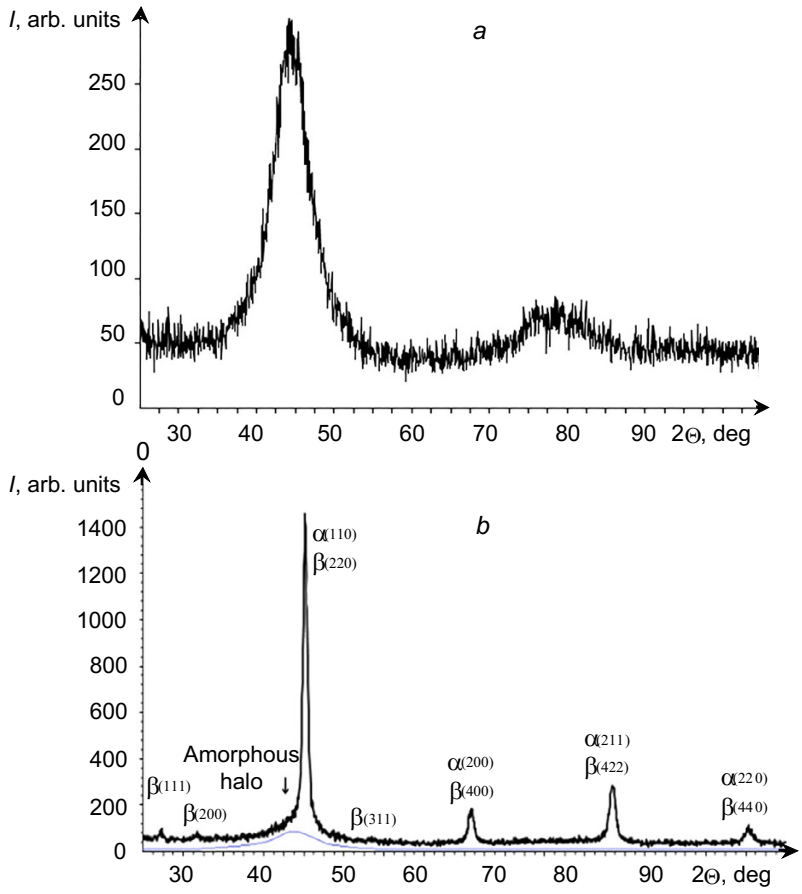

Fig. 1. Diffraction patterns of the $Fe_{72,5}Cu_1Nb_2Mo_{1,5}Si_{14}B_9$ alloy ribbons in the initial quenched state (*a*) and after heat treatment at 570°C, 1 h (*b*), α – α-Fe(Si) solid solution, β – cubic Fe_3Si.

annealing of the initial quenched specimens (without irradiation) at T = 570°C, 1 h, specifically to the solid solution of α-Fe(Si) and Fe_3Si. Furthermore, the form of the diffraction patterns evidences of the presence of an H-phase with the hexagonal symmetry $P6_3/mmc$, which was identified in [21] in the late crystallization phases and after laser irradiation of the finemet alloy. An analysis of the resulting diffraction patterns (taking into account the data on the parameters of well-known crystal structures observed earlier in similar alloys) also indicates, in addition to the Fe_3Si and αFe(Si) phases, a very likely presence of the phases similar to $Fe_{23}B_6$, Fe_5Si_3 and Fe_2B, which is consistent with the data reported in [21–23].

An analysis of the diffraction patterns has demonstrated that the average size of nanocrystallites formed after irradiation is noticeably larger than that after annealing, 35 and 17 nm – for the α-Fe(Si) solid solution and 34 and 19 nm – for Fe_3Si, respectively (Tables 1 and 2). Whether the crystallite size depends on the irradiation conditions requires additional studies.

Similar results were obtained after analyzing the diffraction patterns taken from unirradiated sides of the ribbons. This suggests irradiation-induced crystallization in the entire volume of the 25 μm-thick ribbon.

The analytical results for the irradiated specimens subjected to a subsequent annealing treatment are presented in Table 2. It is clear that as the temperature increases the volume fraction of the crystalline Fe_3Si phase decreases, while the fraction of the α-Fe(Si) solid solution increases, in other words there is an increase in the volume fraction of the crystal phase with a lower content of silicon. This finding is consistent with the data reported in [24], where the decreased content of silicon in the crystalline phase in later crystallization stages was proved. The fraction of the hexagonal H-phase changes but slightly.

TABLE 1. Phase Composition (*V,%*), CSR Size (*d*) and Crystal Lattice Period (*a*) of the $Fe_{72.5}Cu_1Nb_2Mo_{1.5}Si_{14}B_9$ Alloy After Different Treatments (Superfast Liquid Quenching and Subsequent Furnace Annealing at Different Temperatures T_a, 1 h)

T_a, °C	Amorphous component	α-Fe(Si)			Fe_3Si		
	V, %	*V*,%	*d*, nm	*a*, nm	*V*, %	*d*, nm	*a*, nm
Initial quenched ribbon (before annealing)	100	0	–	–	0	–	–
480 (annealing)	100	0	–	–	0	–	–
500 (annealing)	81	100	13	0.2842	0	–	–
520 (annealing)	57	69	17	0.2844	31	19	0.5660
570 (annealing)	39	65	17	0.2842	35	19	0.5660

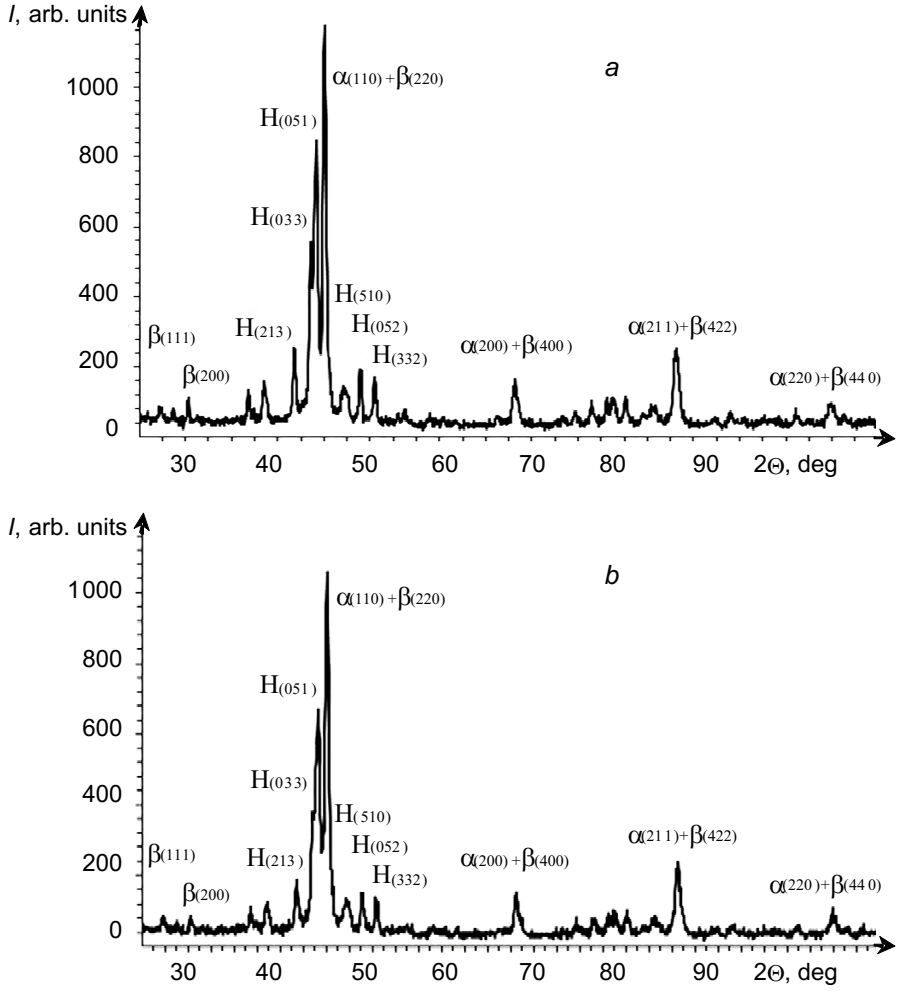

Fig. 2. Diffraction patterns from the $Fe_{72,5}Cu_1Nb_2Mo_{1,5}Si_{14}B_9$ alloy ribbons after irradiation with Ar^+ ions (*a*) and subsequent heat treatment at 570°C, 1 h (*b*), H – hexagonal H-phase, α –α-Fe(Si) solid solution, β – cubic Fe_3Si.

TABLE 2. Phase Composition (*V,%*), CSRs-Size (*d*) and Crystal Lattice Period (*a, c*) of the $Fe_{72.5}Cu_1Nb_2Mo_{1.5}Si_{14}B_9$ Alloy After Different Treatments (Irradiation and Subsequent Furnace Annealing at Different Temperatures T_a, 1 h)

T_a, °C	α-Fe(Si)			Fe_3Si			H-phase		
	V, %	*d*, nm	*a*, nm	*V*,%	*d*, nm	*a*, nm	*V*, %	*d*, nm	*a/c*, nm
Irradiated amorphous ribbon (without annealing)	44	35	0.2848	30	34	0.5678	26	32	1.2291/0.7695
480 (subsequent annealing)	47	36	0.2846	22	37	0.5682	31	37	1.2295/0.7694
520 (annealing)	55	27	0.2845	12	46	0.5702	33	33	1.2301/0.7699
570 (annealing)	58	21	0.2844	12	30	0.5696	30	30	1.2302/0.7695

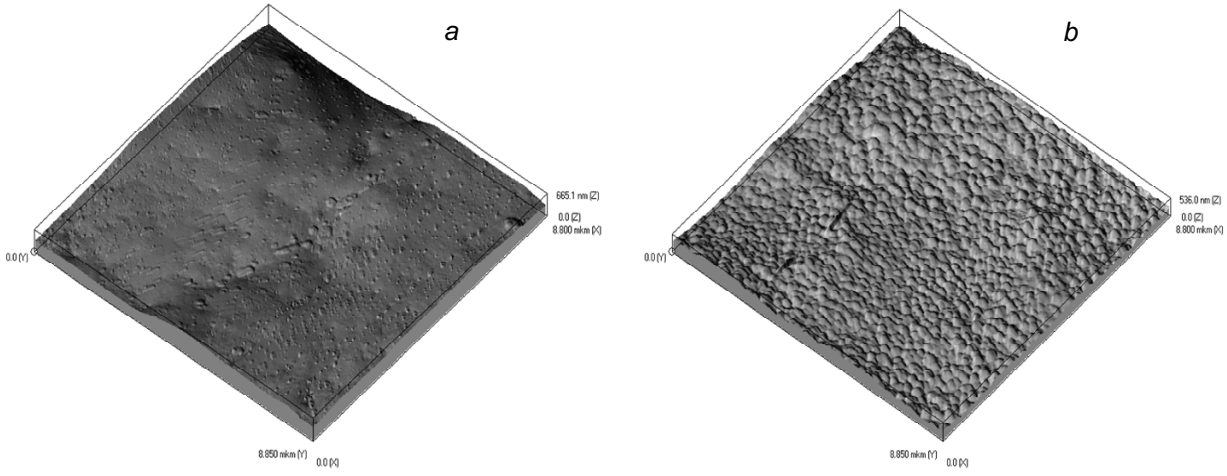

Fig. 3. Relief of the initial amorphous (*a*) and irradiation-crystallized (*b*) $Fe_{72.5}Cu_1Nb_2Mo_{1.5}Si_{14}B_9$ ribbons on the contact (irradiated) side (AFM image, fragment 8.85×8.85 μm).

It should be noted that in the unirradiated specimens a considerable fraction of the crystal phase appears at the temperature 500°C only. At the same time, as a result of irradiation, accompanied by short-duration (~2 s) heating to 350°C, crystallization is observed to take place in the entire volume of the ribbon (we did not determine the lower crystallization temperature bound).

An investigation of the irradiated ribbons using atomic force microscopy (AFM) supported the data on crystallization under the action of short-duration ion irradiation. In particular, an AFM examination in the contact probe interaction with the specimen revealed an evident relief change during crystallization (Fig. 3).

Though the estimate of the average roughness R_a exhibits an insignificant decrease (from 42 to 36 nm), but the relief development, i.e., the differences in heights, increases fourfold (from 0.9 to 3.8%). In other words, the surface acquires a marked segmented shape, which is clearly seen in Fig. 3*b*.

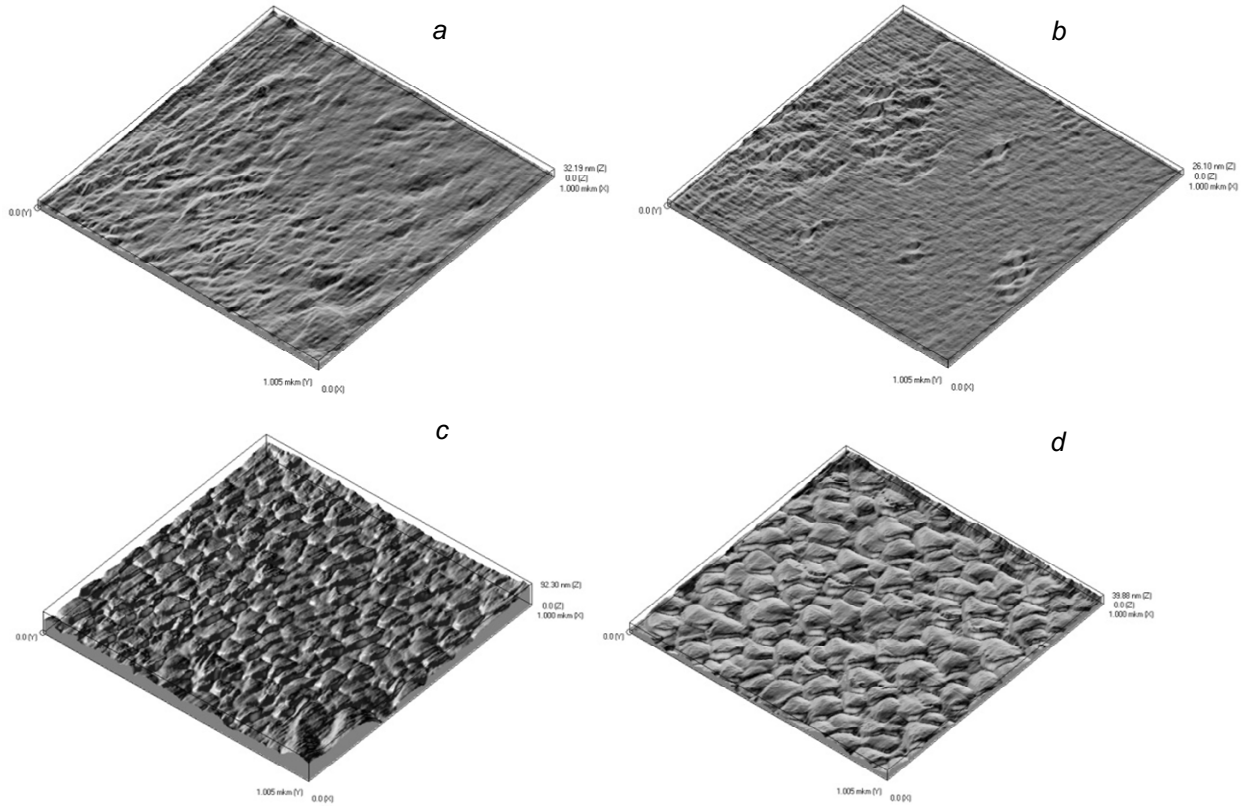

Fig. 4. Relief of the initial amorphous (*a*, *b*) and crystallizing during irradiation (*c*, *d*) $Fe_{72.5}Cu_1Nb_2Mo_{1.5}Si_{14}B_9$ ribbons on both sides: *a*, *b* – contact (irradiated) sides, *c*, *d* – free sides (AFM, fragment 1×1 μm).

For more detailed analysis of the difference between the irradiated and unirradiated ribbon surfaces, an estimation of the relief was performed in the atomic force mode at a higher resolution (Fig. 4).

A small difference in R_a between the sides of the initial amorphous ribbon (2.5 nm compared to 1.2 nm) is accounted for by the conditions of the ribbon production itself, since the contact side, undergoing faster quenching, has a somewhat larger number of structural stresses and hence a more developed relief. Note that as the resolution is increased, R_a decreases, since the objects of smaller dimensionality get into the integral profile over which the calculation is performed. The value of L_0 for both sides is found to be ~0.5%.

After irradiation, the roughness parameter R_a for the irradiated side increases up to 4.5 nm. The relative length L_0 of the profile increases even more significantly: up to 7.2% for the irradiated side and up to 5.1% for the unirradiated side (Fig. 4). This increase indicates an increase in the number of height differences, in other words, surface segmentation.

An analysis of the images presented in Fig. 4 implies that the irradiated and unirradiated surfaces of the 25 μm ribbon undergo marked changes, despite the fact that the average ion penetration depth of accelerated Ar^+ ions is only several tens of nanometers, and the temperature of specimen heating during their irradiation is insufficient for thermal crystallization to occur in the absence of the beam exposure.

Note that the limitations on resolution, specific for the atomic force microscopy, which are determined by the sharpness of the probe, do not allow the size of the crystallites to be determined quantitatively, in particular: what we see in Fig. 4*b*, *d* are not individual grains. These are likely to be grain conglomerates, since the visible dimensions by a factor of 5–10 exceed those obtained from the processed diffraction patterns data.

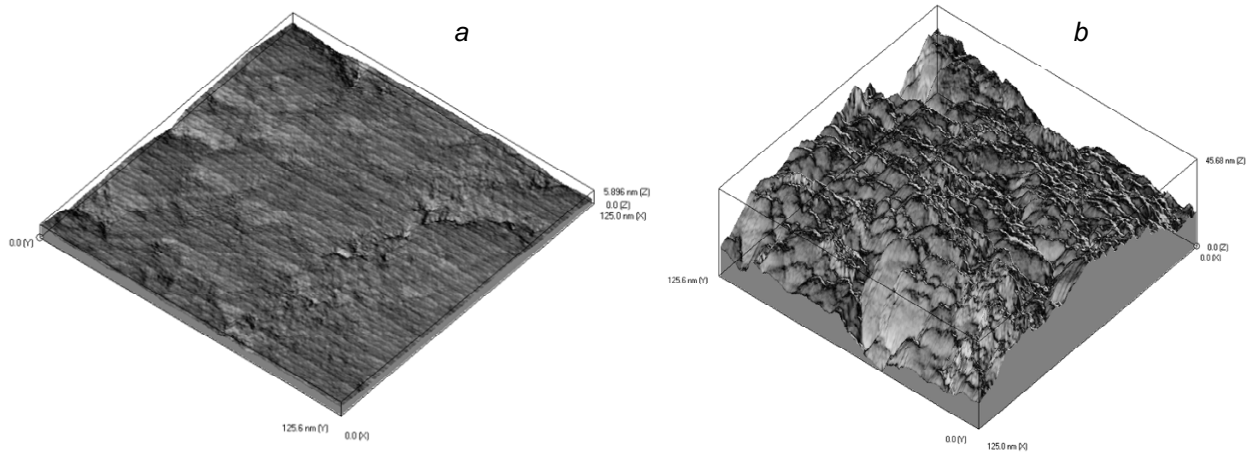

Fig. 5. Relief of the contact side of the amorphous (*a*) $Fe_{72.5}Cu_1Nb_2Mo_{1.5}Si_{14}B_9$ ribbon and that crystallized in the course of ion irradiation (*b*) (STM, fragment 125×125 nm).

In order to clarify the issue of the crystallite size, we resorted to the scanning tunneling microscopy (STM) and investigated both the contact side of the amorphous ribbon and the irradiated contact side of the ribbon crystallized during irradiation.

The images of a higher resolution (Fig. 5) confirm the previous conclusions. It is seen that roughness R_a of the crystallized specimen has increased from 0.57 to 2.3 nm, and the relative profile length ratio L_0 has increased from 1.8 to 29.9%. We can argue that this is a transition from the amorphous to nanocrystalline structure, with the crystallites measuring approximately 10– 12 nm.

CONCLUSIONS

Based on the investigations performed in this study, the following conclusions could be made:

1. The irradiation by Ar^+ ions with the energy 30 keV at the current density 300 μA/cm^2 and the fluence $3.75 \cdot 10^{15}$ cm^{-2} (irradiation time ~2 c) is accompanied by a short-duration heating of the specimens to 350°C (which is 150°C lower than the thermal crystallization threshold), which gives rise to complete crystallization of the amorphous alloy (throughout the entire volume of the 25 μm-thick ribbons), followed by precipitation of crystals of the α-Fe(Si) solid solution, close in its composition to those of $Fe_{80}Si_{20}$, stable Fe_3Si phase, and metastable hexagonal phases.

2. The-irradiation-induced nanocrystallization gives rise to the formation of nanocrystallites, whose size is twice larger than of those formed as a result of furnace annealing; moreover, this is followed by relief changes both on the irradiated and unirradiated surfaces of the $Fe_{72,5}Cu_1Nb_2Mo_{1,5}Si_{14}B_9$ alloy ribbons.

3. The results obtained serve an additional proof of the presence of radiation-dynamic component of the exposure to beams of accelerated ions on metastable media [14]. This is indicated by the process of nanocrystallization of the alloy under study during its short-duration ion-beam heating at the depth significantly exceeding the projected ion range and at the temperature much lower than that of the thermal crystallization threshold.

4. The data obtained in conjunction with the electrical characteristics [12, 15], sensitive to the ion-beam treatment modes, could be useful in designing energy- and cost-effective industrial processes for modification of properties of the class of materials under consideration.

This study has been funded by the Russian Science Foundation (Project No. 15-19-10054).

REFERENCES

1. Yu. I. Golovin, Introduction into Nanotechnology [in Russian] Mashinostroyenie, Moscow (2003).
2. R. A. Andrievskii and A. V. Ragulya, Nanostructured Materials [in Russian], Akademia Publ. Center, Moscow (2005).
3. A. I. Gusev, Nanomaterials, Nanostructures, Nanotechnologies [in Russian], Fizmatlit, Moscow (2005).
4. Nanocrystalline Materials. The Synthesis-Structure-Properties Relationships and Applications (Ed. S. C. Tjong), Elsevier Ltd. (2006).
5. A. N. Didenko, Yu. P. Sharkeev, E. V. Kozlov, and A. I. Ryabchikov, The Effects of Long-Range Action in Ion-Implanted Metallic Materials [in Russian], NTL Publ., Tomsk (2004).
6. R. Z. Valiev and I. V. Aleksandrov, Bulk Nanostructured Metallic Materials: Formation, Structure and Properties [in Russian], IKTs Akademkniga (2007).
7. R. A. Andrievskii and A. M. Glaezer, Usp. Fiz. Nauk, **179**, Iss. 4, 337–358 (2009).
8. A. M. Glaezer, Deform. Razrush. Mater., No. 2, 1–7 (2010).
9. S. P. Bugaev, A. M. Iskoldskii, G. A. Mesyats, and D. I. Proskurovsky, Sov. Tech. Phys., **37**, Iss. 12, 2206–2208 (1967).
10. Plasma-Emitter Sources of Charged Particles (Ed. P. M. Schanin) [in Russian], Nauka, Ekaterinburg (1993).
11. V. V. Ovchinnikov, V. I. Chernoborodov, and Yu. G. Ignatenko, Nucl. Instrum. Methods Phys. Res. B, **103**, 313–317 (1995).
12. B. K. Sokolov, V. V. Gubernatorov, Yu. N. Dragoshanskii, *et al*., Phys. Met. Metallogr., **8**9, Iss. 4, 348–357 (2000).
13. V. V. Ovchinnikov, N. V. Gavrilov, N. V. Gushchina, *et al*., Russ. Metallurg. (Metally), No. 2, 62– 69 (2010).
14. V. V. Ovchinnikov, Phys. Usp., **51,** Iss. 9, 955–974 (2008).
15. V. V. Gubernatorov, Yu. N. Dragoshanskii, V. A. Ivchenko, V. V. Ovbchinnikov, and T. S. Sycheva, A method for thermomagnetic processing of magnetically soft materials, RF Patent No. 2321644, MPK C21D 1/04 (2006.01); applicant and patent holder: Institute of Metal Physics UB RAS No. 2006128319/02; Appl. 03.08.06; Publ. 10.04.08, Bull. No. 10 (2008).
16. V. V. Ovchinnikov, V. N.Chernoborodov, E. P. Mikhalishcheva, *et al*., Trans. Mat. Res. Soc. Jpn., **16B**, 1489–1492 (1994).
17. V. V. Ovchinnikov, N. V. Gushchina, T. M. Gapontseva, *et al*., High Pressure Res., No. 5, 1–10 (2015).
18. G. Herze, IEEE Trans. Magn., **2**5, 3327–3329 (1989).
19. Y. Yoshizawa, Nanocrystalline soft magnetic materials and their applications, in Handbook of Advanced Magnetic Materials 4: Properties and Applications (Eds. by Y. Liu, D. J. Sellmyer, and D. Shindo) Springer, New York (2006).
20. N. V. Gavrilov, G. A. Mesyats, S. P. Nikulin, *et al*., J. Vac. Sci. Technol., **A14,** 1050–1055 (1996).
21. I. V. Lyasotskii, N. B. Dyakonova, E. N. Vlasova, *et al*., Phys. Stat. Sol. A, **203**, 259–270 (2006).
22. G. Rizza, A. Dunlop, G. Jaskierowicz, and M. Kopcewicz, Nucl. Instrum. Methods Phys. Res. B, **2**26, 609–621 (2004).
23. N. V. Mushnikov, A. P. Potapov, D. A. Shishkin, *et al*., Phys. Met. Metallogr., **116**, No. 7, 663–670 (2015).
24. J. M. Borrego, C. F. Conde, and A. Conde, Phil. Mag. Lett., **80**, 359–365 (2000).